

Melting behavior of quasi-two-dimensional N₂ adlayers deposited on graphite

Bogdan Kuchta* and R. D. Etters

Department of Physics, Colorado State University, Fort Collins, Colorado 80523

(Received 20 March 1995; revised manuscript received 3 May 1996)

The melting behavior of partial and complete N₂ monolayers on graphite is examined using a Monte Carlo procedure in conjunction with the multiple histogram method. It is found that vacancies inherent in partial monolayers, and those thermally induced by out-of-plane motion at or near monolayer completion, are important factors in predicting the density dependence of the melting temperature. Calculated at various surface densities are the melting temperatures, specific heats, order parameters, probability distributions for molecular positions and orientations, and fluctuations in these quantities. With this information the mechanism of the melting transition is elucidated, and the temperature and density dependence of the specific heats and order parameters is explained. [S0163-1829(96)00241-X]

I. INTRODUCTION

Physisorbed adlayers deposited on graphite have provided an opportunity to examine the melting behavior of nearly two-dimensional (2D) systems. This feature has been exploited both experimentally and theoretically.^{1,2} Most theories are based upon the notion that melting is promoted by dislocations, vacancies, grain boundaries, impurities, and other such imperfections. This is not surprising since the above phenomena deplete the crystalline order that vanishes upon melting. Much considered among the general theories² of 2D melting has been the dislocation mediated theory of Kosterlitz, Thouless, Halperin, Nelson, and Young.³ One possible outcome involves two second-order transitions. The first is from the solid into a hexatic phase where the vectors connecting molecular mass centers to their nearest neighbors exhibit sixfold azimuthal symmetry. The second is from the hexatic phase into an isotropic fluid. Evidence supporting this prediction remains controversial. Many other calculations⁴⁻¹⁵ on model and physical systems have provided insight into the nature of the melting transition. It is noted that assumptions utilized in various theories can importantly change the interpretation of results. Constraints of strict two-dimensionality, neglect of some crystalline imperfections, the suppression of certain degrees of freedom, the nature of the boundary conditions, etc., can compromise our ability to understand the behavior of quasi-2D systems.

For N₂ adlayers deposited on graphite, low-energy electron diffraction (LEED),¹⁶⁻²⁰ heat capacity,²¹⁻²³ neutron diffraction,^{24,25} calorimetry,^{22,26,27} and vapor pressure measurements²² have provided a fairly detailed description at adlayer densities $\rho \leq 1$, where the upper limit refers to the complete monolayer. At $\rho = 1$ the mass centers form a $\sqrt{3} \times \sqrt{3}$ registered lattice that persists until melting.²⁴ For $\rho < 1$, scattering data^{24,25} also shows evidence of the same structure until melting. This strongly implies the existence of $\sqrt{3} \times \sqrt{3}$ islands separated by vacancies and voids. Experimental data supporting this possibility are not, however, exhaustive. Nevertheless, recent calculations for N₂ clusters on graphite support experiment. At $T_{OD} \approx 27$ K, an orientational order-disorder transition occurs,^{17,28} which is nearly independent of surface density ρ . Below T_{OD} the N₂ molecules form an in-

plane herringbone arrangement^{17,18} and above they act as weakly hindered, nearly planar rotors. The melting temperature is observed^{16,21,22,24} to be nearly constant at approximately 47 K, for $0.2 < \rho \leq 0.8$. For $\rho < 0.2$, the only measured value for T_M is noticeably lower, although there is considerable uncertainty about its accuracy. For $\rho \geq 0.8$, T_M rapidly increases with density to a value of approximately 83 K at $\rho = 1$. This feature is qualitatively common to numerous other adlayers deposited on graphite.^{2,29-33}

There have been several calculations directed specifically at the melting of N₂ on graphite. Joshi and Tildesley³⁴ used a molecular dynamics (MD) simulation with 140 molecules based upon a rectangular starting configuration in which a strip occupying half of the MD cell was populated in the $\sqrt{3} \times \sqrt{3}$ structure. Periodic boundary conditions commensurate with this structure were imposed in one direction and free surface boundary conditions in the other. Lennard Jones 6-12 expressions were used for the N₂-N₂ and N₂-substrate potentials. Image charge and substrate-mediated dispersion interactions were neglected. They obtained a melting temperature $T_M \approx 39$ K, but, with the improved modification of the substrate interaction by Carlos and Cole,³⁵ they predicted 45 K. Other experiments³⁶ and calculations, such as MD (Ref. 37) and renormalization theory,³⁸ are especially relevant to this problem.

In earlier work³⁹ we showed that a complete N₂ monolayer, subject to constant surface area boundary conditions, would melt at about 85 K. The transition was accompanied with a sharp increase of translational fluctuations normal to the substrate plane, despite strong normal forces that bind the N₂ molecules to the substrate. But there was no signature at melting from fluctuations in the substrate plane. Upon replacing this boundary condition with one of constant pressure, the monolayer melted at 45 K. Unlike the previous case, fluctuations normal to the substrate do not signal the transition but those in the substrate plane increase sharply at melting. Because that work was limited to the response of monolayers only, these results are directed to calculations to partial N₂ layers with $0.2 \leq \rho \leq 1.0$. A part of these results have been reported in an earlier work.⁴⁰ Among the observations was evidence of second-layer promotion near T_m at $\rho = 1$. It is noteworthy that Koch and Abraham⁶ identified an

increase in second-layer population of Xe atoms with increasing temperature at $T > T_M$. As will be explained later, this feature is important in understanding the dynamics of monolayer melting. The goal of this work is to present various results not shown in the earlier work, and interpret them in terms of physical processes.

II. METHOD AND INTERACTIONS

In selecting a method of calculation for melting over a range of N_2 surface densities $0 \leq \rho \leq 1$, it is important to recognize that all lattice sites of the complete monolayer are occupied at low temperatures, and near melting only thermally activated vacancies in this structure are possible. However, for $\rho < 1$, there are more lattice sites than molecules to occupy them. This means that vacancies exist in the adlayer plane even at the lowest temperatures. To emulate this important feature a Monte Carlo method was employed with an (N, ρ, T) ensemble and periodic boundary conditions. The number of N_2 molecules in the MC cell that contains $m \sqrt{3} \times \sqrt{3}$ lattice sites is N . Thus, $\rho = N/m$. Calculations have been made at $\rho = 1.0, 0.95, 0.93, 0.9, 0.5$, and 0.2 . For each density m is chosen so that proper boundary conditions can be satisfied and N is at or near 256. The $m-N$ vacancies are initially introduced by randomly locating them at various sites of the $\sqrt{3} \times \sqrt{3}$ lattice. They can appear as point defects in an otherwise perfect structure or as an aggregation of vacancies, called voids. For each density, calculations are performed at eight different temperatures. At each point probability distributions are calculated from approximately 5×10^5 steps, after about half that many are discarded to minimize initial transients. Each step consists of random movement of all $5N$ degrees of freedom. These distributions are then employed in a multiple histogram method^{41,42} that facilitates the determination of accurate thermal averages.

The histogram method takes advantage of the width of the probability distribution around a given thermodynamic point to gain information at neighboring points. To see how the distribution at one point can be used to determine it at another, recall that

$$P_\beta(E) = N_\beta(E)/n_\beta = W(E) \exp[-\beta E + f], \quad (1)$$

where the probability distribution is $P_\beta(E)$, the temperature is $\beta = (kT)^{-1}$, $W(E)$ is the density of states at energy E , and $F = f/\beta$ is the Helmholtz free energy. In a Monte Carlo calculation $N_\beta(E)$ is the number of accepted configurations in the interval E to $E + \Delta E$ out of n_β total configurations. Note that in equilibrium $P_\beta(E)$ peaks at some energy and tails off away from this value. It is these tails that give information at energies relevant to neighboring points β' . Here temperature is used to identify the thermodynamic points, but other variables may be useful alternatives. As pointed out by Ferrenberg and Swendsen,⁴¹ $P_{\beta'}(E)$ is mathematically related to $P_\beta(E)$ by the exact expression

$$P_{\beta'}(E) = \frac{P_\beta(E) \exp[-(\beta' - \beta)E]}{\sum_E P_\beta(E) \exp[-(\beta' - \beta)E]}. \quad (2)$$

An examination of the numerator shows that $P_{\beta'}(E)$ is most accurate when $|\beta' - \beta|$ is small and $P_\beta(E)$ is broad and well described. Clearly, these are reasonable expectations.

The multiple histogram method⁴² is a straightforward generalization of the above-mentioned arguments. If Monte Carlo calculations are performed at R different temperatures, the normalized probability distribution is

$$P_\beta(E) = D_\beta(E) / \sum_E D_\beta(E), \quad (3)$$

$$D_\beta(E) = \frac{\sum_{i=1}^R N_i(E)}{\sum_{i=1}^R n_i \exp[-(\beta_i - \beta)E + f_i]}, \quad (4)$$

where

$$\sum_E D_{\beta_i}(E) = \exp(-f_i). \quad (5)$$

Clearly Eq. (5) is simply the partition function (normalization) for $P_{\beta_i}(E)$. The free energies $\{f_i\}$, $i = 1, 2, \dots, R$, can be determined self-consistently from Eqs. (3) and (4), or from the intersection of neighboring histograms $\{N_i(E)\}$. That is,

$$P_{\beta_i}(E)/P_{\beta_{i+1}}(E) = \exp[-(\beta_i - \beta_{i+1})E + (f_i - f_{i+1})].$$

If these distributions overlap, there is one energy \bar{E} where $P_{\beta_i}(\bar{E}) = P_{\beta_{i+1}}(\bar{E})$. Then

$$f_i - f_{i+1} = (\beta_i - \beta_{i+1})\bar{E}. \quad (6)$$

It is sufficient to determine the set $\{f_i\}$ to within an additive constant so one value is set equal to zero and all others are measured with respect to it. It is noted that the multiple histogram method is equal to or better than separate calculations initiated at the points studied. When the probability distributions of these points overlap, the gain can be very substantial. As will be described, this is important here because of the large computational requirements of the problem.

The interactions between N_2 molecules are represented by our site-site fit to *ab initio* results of Berns and van der Avoird,⁴³ and the Gordon-Kim electron gas results of LaSar⁴⁴ at small separations. This expression, which includes a point charge representation of the electric multipole interactions, has proved to be highly accurate in representing 3D N_2 in the solid, fluid, and gaseous phases over a wide range of (T, P) ,⁴⁵⁻⁴⁷ including the characterization of solid-solid and solid-fluid phase transitions. Moreover, it has proved reliable in characterizing N_2 on graphite,^{48,49} including the orientational order-disorder transition.⁴⁹ The interaction between ad molecules and the substrate is composed of several terms. There is the overlap-dispersion interaction between the carbon and nitrogen atoms that is described by a Lennard Jones (6-12) potential. The potential parameters $(\sigma, \epsilon) = (3.36 \text{ \AA}, 31 \text{ K})$ are those deduced by Steele.⁵⁰ It is represented by a Fourier expansion.⁵¹ The second term in that expansion, which reflects the periodicity of the substrate- N_2 interaction, is given by the representation of Carlos and Cole.³⁵ In addition, there are the Coulomb interactions between charges representing the N_2 multipoles and their images induced in the graphite substrate, and the substrate-mediated dispersion expression that depends on the graphite dielectric function and the dynamic polarizability of the N_2 ad molecules. Calculations for $T_M(\rho)$ are presented using this latter potential term and without, for comparison purposes. All other results

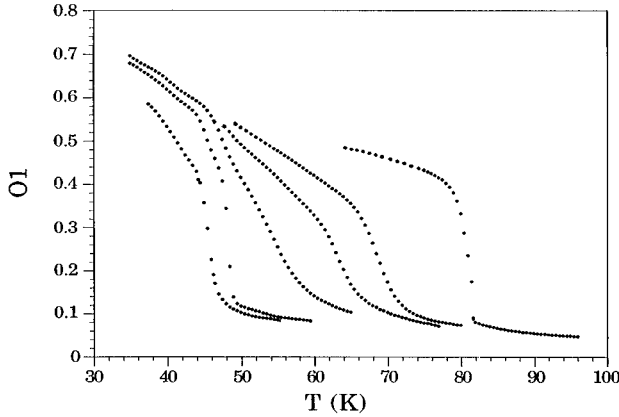


FIG. 1. The order parameter $O1$ vs temperature. The curves, from right to left, are for surface densities $\rho=1.0, 0.95, 0.93, 0.9, 0.5,$ and $0.2,$ respectively.

are presented without it. A discussion of this controversial term is given in Sec. IV. Details and references to all the interactions are given in Ref. 52.

III. RESULTS

The melting transition is signaled by the order parameters $O1$ and $O2$, and the specific heats. A feature in common with them is that they exhibit nonmonotonic behavior with respect to ρ :

$$O1 = 6N^{-1} \sum_{i=1}^N \left\langle \sum_{s=1}^6 \exp(i\mathbf{g}_s \cdot \mathbf{r}_i) \right\rangle, \quad (7)$$

$$O2 = [3N(N-1)]^{-1} \sum_{i < j}^N \left\langle \sum_{s=1}^6 \exp(i\mathbf{k}_s \cdot \mathbf{r}_{ij}) \right\rangle, \quad (8)$$

where \mathbf{g}_s and \mathbf{k}_s are the primitive reciprocal-lattice vectors of the graphite surface and the $\sqrt{3} \times \sqrt{3}$ structure, respectively. Here the $\{\mathbf{r}_{ij}\}$ locate mass center positions of the N_2 molecules in the substrate (x, y) plane, and $\mathbf{r}_{ij} = \mathbf{r}_i - \mathbf{r}_j$. Note that $O1$ is simply the structure factor evaluated at the primitive reciprocal-lattice vectors of the substrate. It equals unity if all N_2 mass centers are statically located over the center of a graphite hexagon and zero if they uniformly sample all positions. Similarly, $O2$ is unity for a $\sqrt{3} \times \sqrt{3}$ structure and zero if there is no vestige of it. Figure 1 shows $O1$ versus temperature. The curves are for $\rho=1.0, 0.95, 0.93, 0.9, 0.5,$ and $0.2,$ from right to left, respectively. There are several noteworthy features. At each density there is a small temperature interval where $O1$ reduces rapidly from relatively large values to very small. Thus, at temperatures below this interval the probability for locating N_2 centers above the center of graphite hexagons is high, and above it is low. However, the high-temperature tail in $O1$ indicates that there is some preference for the molecules to be over the center of a graphite hexagon, even well above the transition. This is understandable since the center of a graphite hexagon is a potential energy minimum for a single N_2 ad molecule. The fluid is modulated by this minimum. Note that the sharpness of the transition signaled by $O1$, and other features, vary consider-

ably and in a nonmonotonic way with changing density ρ . These features reveal information about the dynamics of melting, and will be discussed in Sec. IV. In Ref. 40, 02 shows similar features as $O1$, except that there is no high-temperature tail, indicating the absence of $\sqrt{3} \times \sqrt{3}$ order above the transition.

The calculated specific heat, in units of Nk_B , is shown in Fig. 2(a) versus temperature for $\rho=1.0, 0.95,$ and $0.93,$ from top to bottom, respectively. In Fig. 2(b) are the results for $\rho=0.9, 0.5,$ and $0.2.$ The large number of calculated temperature points at each density is a consequence of the multiple histogram method that gives a continuous map of physical properties versus temperature. These results agree well with experiment,²¹⁻²³ both qualitatively and quantitatively. For example, the nonmonotonic change in the specific-heat peaks and widths with ρ are observed both here and in experiment. These features expose the character of the transition, as will be discussed in Sec. IV. Note that a qualitative figure of the peaks at $\rho=1.0$ and 0.95 are in Ref. 40.

The calculated order parameters and the specific heats all signal transitions at virtually identical temperatures, $T_M(\rho)$, for the various values of ρ . These values are plotted on Fig. 3 and are shown as solid circles with flags representing the statistical uncertainty. The other points represent experimental data^{21,22} for the melting curve, except the crosses which will be explained later. The calculated transitions at $T_m(\rho)$ cannot be completely identified as melting just from the specific heats and the order parameters. For example, an commensurate-incommensurate transition, or an amorphous phase, could show similar results. Thus, several tests were conducted to confirm melting. First, a few N_2 molecules were targeted and their trajectories were monitored along the MC sequences. Below T_M they generally fluctuate about their $\sqrt{3} \times \sqrt{3}$ lattice sites, although occasionally they would migrate from one lattice site to another. Above T_M these molecules migrate easily over the entire surface. Additionally, an examination of the pair-distribution function showed distinct $\sqrt{3} \times \sqrt{3}$ peaks below T_M , and diffuse fluidlike behavior above. In the latter case, however, the distribution showed some departure from ideal fluid behavior. The calculated order parameters and specific-heat peaks not only predict accurately the observed melting curve, as shown in Fig. 3, but their nonmonotonic change in behavior with ρ strongly suggests that the character of melting changes as well. The source of this feature will be discussed in Sec. IV.

Figures 4–8 show instantaneous configurations of the N_2 mass centers projected onto the substrate plane. The format is as follows. Figures are shown for five different surface densities, each at three different temperatures. The temperatures are chosen to be below, near, and above the transition. Each configuration shown is selected from those along the Monte Carlo sequence that are already equilibrated so, in that sense, they can be regarded as typical. While the vacancies and other imperfections are somewhat mobile along the sequence at higher temperatures, all configurations for a given (ρ, T) are very similar. Figure 4 shows equilibrium configurations for $\rho=1$. At $T=75$ K, some 7 K below the transition, the configuration exhibits predominantly the $\sqrt{3} \times \sqrt{3}$ structure, but not perfectly. Some vacancies and dislocations exist in the monolayer plane. As will be discussed, they occur primarily by thermally activated second layer pro-

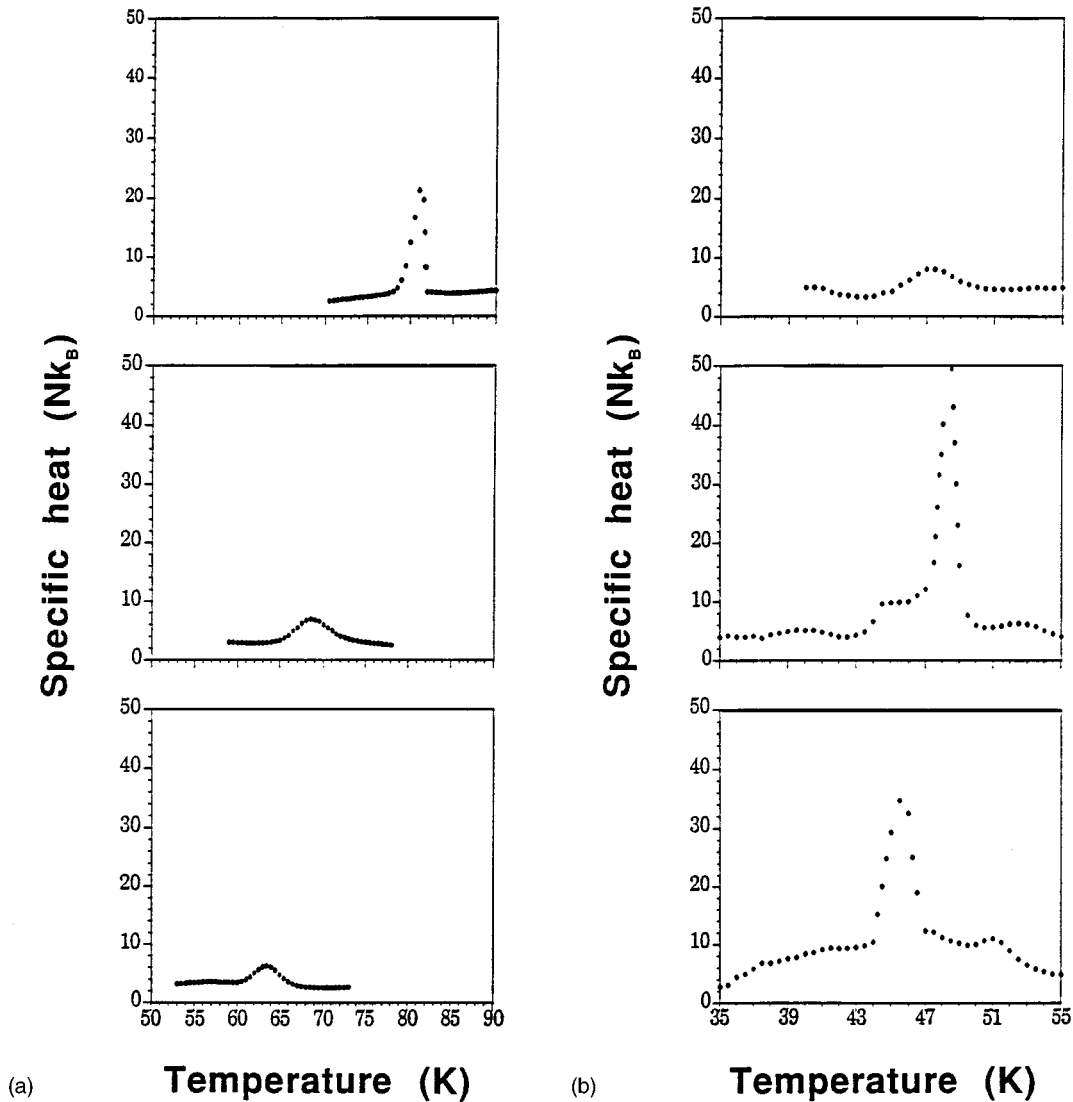


FIG. 2. (a) The specific heat vs temperature for surface densities $\rho=(1.0, 0.95, 0.93)$, from top to bottom, respectively. (b) The specific heat vs temperature for $\rho=(0.9, 0.5, 0.2)$, from top to bottom, respectively.

motion. At $T=82$ K, very close to the transition, the configuration shows a substantial loss of crystalline order and the number of vacancies and dislocations are increased compared to 75 K. At 95 K, some 13 K above the transition, the disorder is nearly complete. Also, by tagging individual molecules and following them along a Monte Carlo trajectory, it is evident that they almost uniformly sample all positions in the substrate plane.

Figure 5 shows configurations for $\rho=0.95$, where 5% of the $\sqrt{3}\times\sqrt{3}$ lattice sites are initially vacant. As such this system is fundamentally different than the above-discussed case for the complete monolayer, where no vacancies are introduced into the initial state. At 55 K, some 12 K below the transition, the vacancies tend to coalesce into voids, around which are dislocations and other distortions in an otherwise $\sqrt{3}\times\sqrt{3}$ structure. At 67 K, very near the transition, the voids are less pronounced and the $\sqrt{3}\times\sqrt{3}$ order is less distinct than at 55 K. At 80 K, some 12 K above melting, the disorder is evident and there is not much second-layer promotion.

Figure 6 shows configurations for $\rho=0.9$. At 35 K the structural order is very pronounced, even near the large voids

that form. At 47 K, slightly below melting, the voids become smaller but create local distortions from the otherwise $\sqrt{3}\times\sqrt{3}$ order. At 55 K structural disorder is evident.

Figure 7 shows configurations for $\rho=0.5$. We chose for an initial configuration a rectangular strip covering exactly one-half the MC cell, with all $\sqrt{3}\times\sqrt{3}$ sites occupied. Sites in the other half were initially unoccupied. At 35 K the $\sqrt{3}\times\sqrt{3}$ order is evident, even near the edges which have developed an uneven boundary. Very near melting, at 48 K, rearrangements and disorder are more noticeable. At 56 K, there is a pattern of structural disorder with large voids in between more densely populated regions. Figure 8 shows results for $\rho=0.2$. At 38 K, about 8 K below the transition, a single $\sqrt{3}\times\sqrt{3}$ island is observed. Just above melting at 48 K, the order has broken down although some clustering between large voids is evident. At 55 K, the configuration is similar to that at 48 K but there is considerably more disorder.

In Fig. 9 is the probability distribution $P(\theta)$ for the polar angle θ , which defines the orientation of the N_2 molecules with respect to the z axis, normal to the substrate plane. For densities $\rho=1.0, 0.95, 0.9$, and 0.2 , the solid and open circles

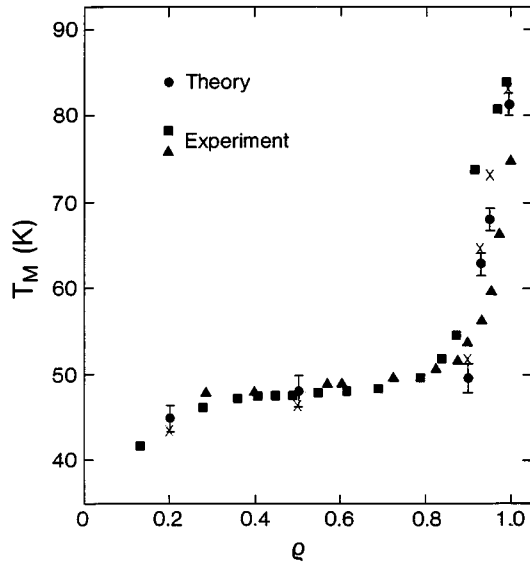


FIG. 3. The circles show the calculated melting temperatures vs surface density and the flags represent the statistical uncertainty. The squares [22] and the triangles [21] show experimental results. The crosses represent calculations that include the substrate-mediated dispersion term (Ref. 53) of the adlayer-substrate interaction.

represent $P(\theta)$ for temperatures (75, 95 K), (55, 80 K), (35, 55 K), and (38, 55 K), respectively. The two temperatures selected for each density span the melting transition. Note that the peaks show a propensity for molecules to orient in the substrate plane, and their width is a measure of the orientational fluctuations about equilibrium. Notable about the distributions are their wings, particularly at $\rho=1.0$ and 0.95. They occur because there is a significant probability for the N_2 molecules to be oriented nearly normal to the substrate. This is easily deduced by plotting the distribution versus $\cos\theta$ rather θ . Then the abscissa is uniform with respect to the probability in an orientational interval, as shown for $\rho=1$ in the second of Ref. 39. Temperature is dominant in influencing the shape of the distributions, rather than the density ρ . Notice that the distributions are not sensitive to the phase of the adlayer.

The rms fluctuations of the N_2 mass centers about their mean positions normal to the substrate plane are shown versus temperature in Fig. 10. It is given by $\langle(\Delta z)^2\rangle^{1/2}$, where $\Delta z = z - \langle z \rangle$. This quantity increases linearly with temperature and is independent of surface density for $T < 70$ K. The paucity of data at higher temperatures for $\rho < 0.93$ eliminates the possibility of predicting its behavior above 70 K but, for $\rho > 0.93$, the fluctuations depart dramatically from the low-temperature linear dependence. There is no evidence that the fluctuations are sensitive to the phase of the adlayer. In previous work³⁹ it was reported that the normal fluctuations at $\rho=1$ exhibit a cusp at $T \approx 87$ K. This was an artifact caused by a peculiar and incorrect way of defining $\langle(\Delta z)^2\rangle$.

The substrate-mediated dispersion was omitted in Refs. 39 and 40, despite claims to the contrary. This occurred because of an unintended alteration of the program. Actually, use of this correction to the adlayer-substrate interaction creates a problem. It is physically warranted, but the approxi-

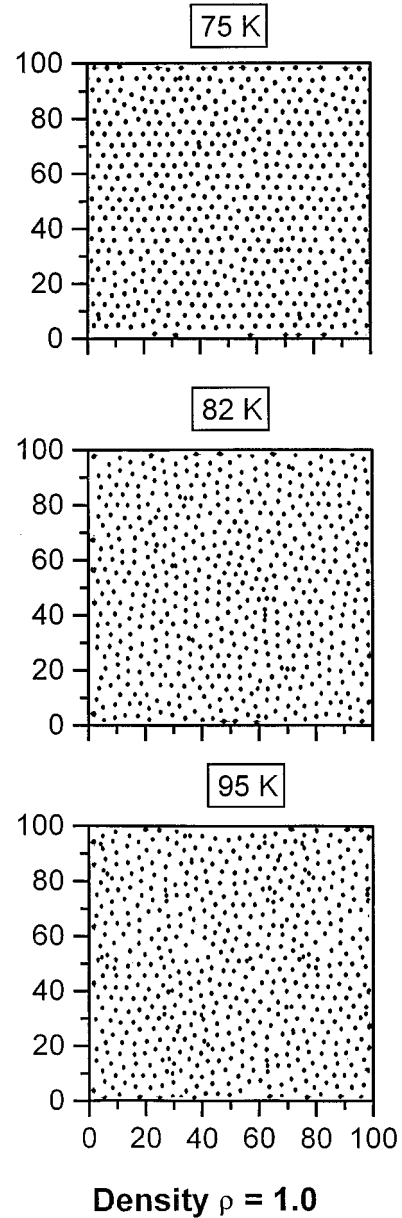


FIG. 4. Typical equilibrium configurations of N_2 mass centers for temperatures 75, 82, and 95 K, at $\rho=1$. Units are in \AA .

mate method used to calculate its strength is not very reliable.^{53,54} Moreover, this term must be damped out as the electron distributions between two molecules overlap, where it is invalid. The character of the damping is unknown. Nevertheless, it is prudent to determine the contribution of this term to physical properties, if only to gauge the uncertainty of the results. The atom-atom coefficients C_{1s} and C_{2s} are from Ref. 55. All features of the work were unchanged qualitatively, but there were modest quantitative changes. In Fig. 3 the cross symbols show the predicted melting temperatures versus ρ , with the substrate-mediated term included. As can be seen, the agreement between these results and experiment remains satisfactory.

IV. SUMMARY AND DISCUSSION

The calculated specific heats and order parameters have given the melting temperatures versus surface density ρ , as

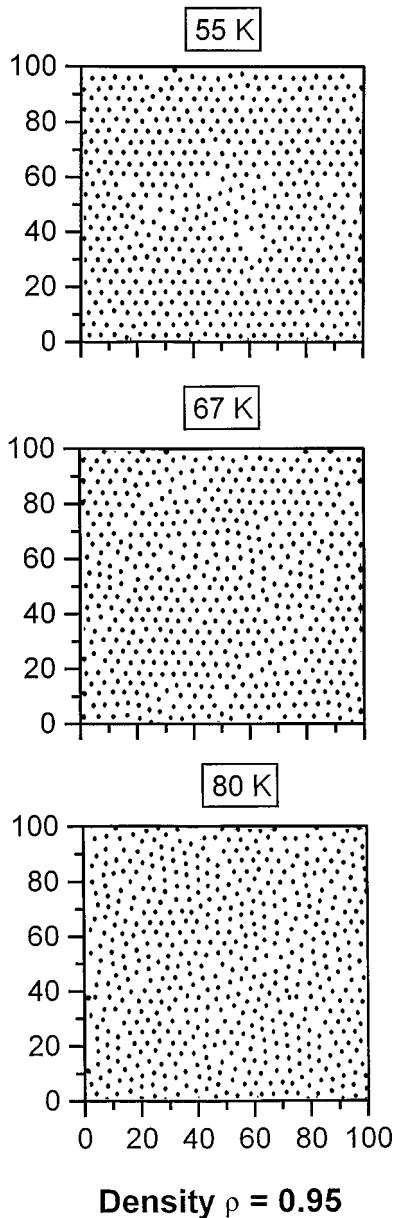


FIG. 5. Typical equilibrium configurations of N_2 mass centers for temperatures at 55, 67, and 80 K, $\rho=0.95$. Units are in Å.

shown in Fig. 3. The comparison with experiment is good.^{21,22} It remains to explain the physical features that contribute to this behavior. It is evident that the value of $T_m(\rho)$ depends upon the number of vacancies in the substrate plane since this is the only thing changed as ρ is changed. At $\rho=1$ all sites are occupied at low temperature and there is insufficient thermal energy to create them until nearly 82 K, the melting temperature. The vacancies occur primarily from second-layer promotion, as demonstrated in Fig. 5 of Ref. 40. This creates vacancies and imperfections in the monolayer that facilitate melting. The role of fluctuations normal to the plane and the second-layer promotions was tested by constraining the ad molecules to be strictly two dimensional. Melting occurred at 13 K higher with the constraint. Also note that the rms center-of-mass fluctuations about equilibrium, normal to the substrate, increase dramatically at $T_M(\rho)$. The in-plane fluctuations show no signature of the

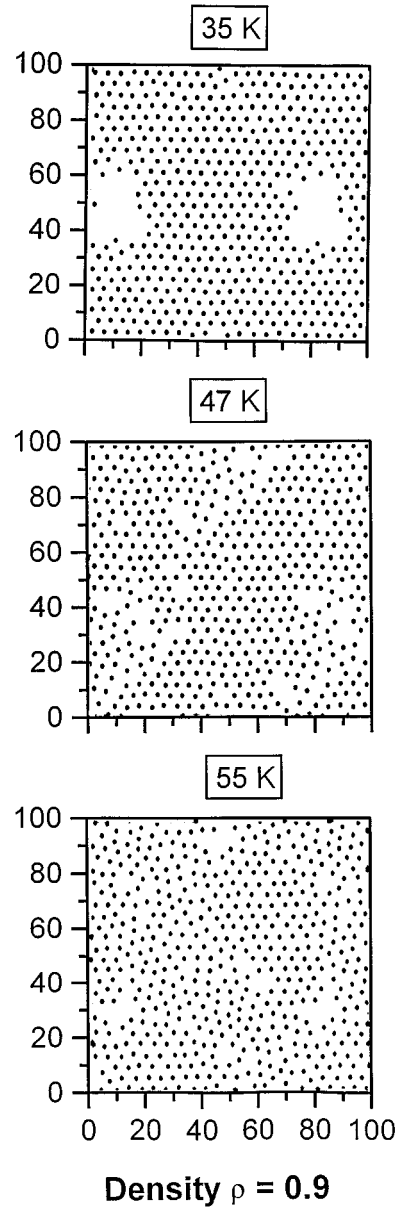


FIG. 6. Typical equilibrium configurations of N_2 mass centers for temperatures 35, 47, and 55 K, at $\rho=0.9$. Units are in Å.

transition. As ρ decreases from unity, the melting temperature decreases rapidly. This can be understood by recognizing that for partially monolayers all lattice sites cannot be occupied. Thus, these vacancies are an intrinsic feature of the system, even in the absence of thermal activation. The molecules near the vacancies, and the voids formed from them, are less bound than others because their coordination number is less. Thus, self-diffusion and melting occurs at temperatures less than at $\rho=1$. At $\rho<0.9$, $T_M(\rho)$ stabilizes at about 47 K, some 35 K below that of the complete monolayer. This result is consistent with the constant pressure calculation³⁹ for a monolayer, where the N_2 surface density responds to a changing thermodynamic environment. At 47 K the adlayer expands, creating vacancies, and melts. At $\rho<0.9$ there is no evidence of vacancy creation in the monolayer plane from thermal excitations out of plane, at $T_M(\rho)$ and well beyond. This is supported by the behavior of $\langle(\Delta Z)^2\rangle^{1/2}$, shown in

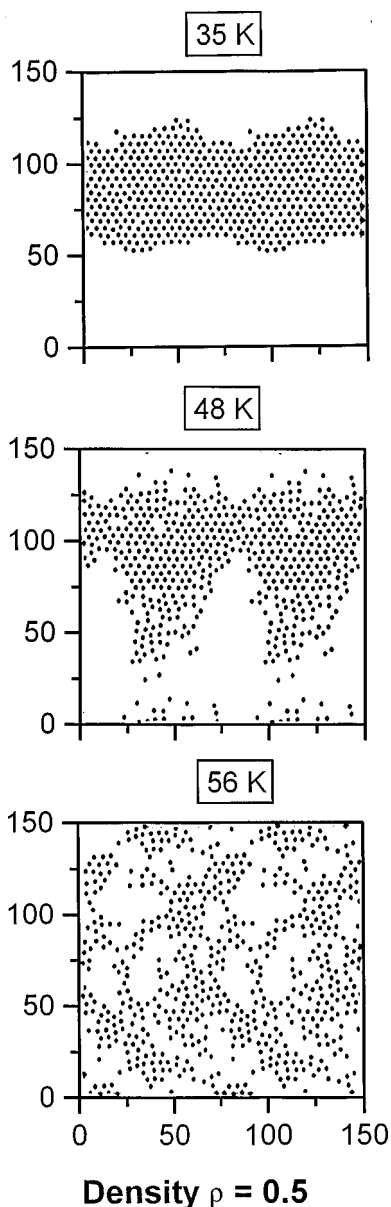


FIG. 7. Typical equilibrium configurations of N_2 mass centers for temperatures 35, 48, and 56 K, at $\rho=0.5$. Units are in Å.

Fig. 10, and from the probability distribution⁴⁰ of molecular centers at a distance Z above the substrate that shows no evidence of second-layer formation. Thus, it is the intrinsic in-plane vacancy population that promotes melting at relatively low temperatures. Because of the strong holding forces, normal to the plane, the temperature at melting is not sufficient to thermally activate significant numbers of vacancies. For $\rho < 0.3$, experiment^{21,22} suggests that T_M lowers below 47 K, as indicated by our calculated point at $\rho=0.2$. However, this conclusion is experimentally supported only by a single point at $\rho < 0.2$, and it is questionable accuracy. Computational data is also too sparse to show a trend. As with experimental evidence,^{24,25} calculation shows that $\sqrt{3} \times \sqrt{3}$ islands form below T_m and $\rho \ll 1$. This is in accordance with previous calculations⁵⁶ on N_2 clusters on graphite. In the limit $\rho \rightarrow 0$, $N \rightarrow \infty$, macroscopic islands are expected^{39,56} at low temperatures because this configuration minimizes the

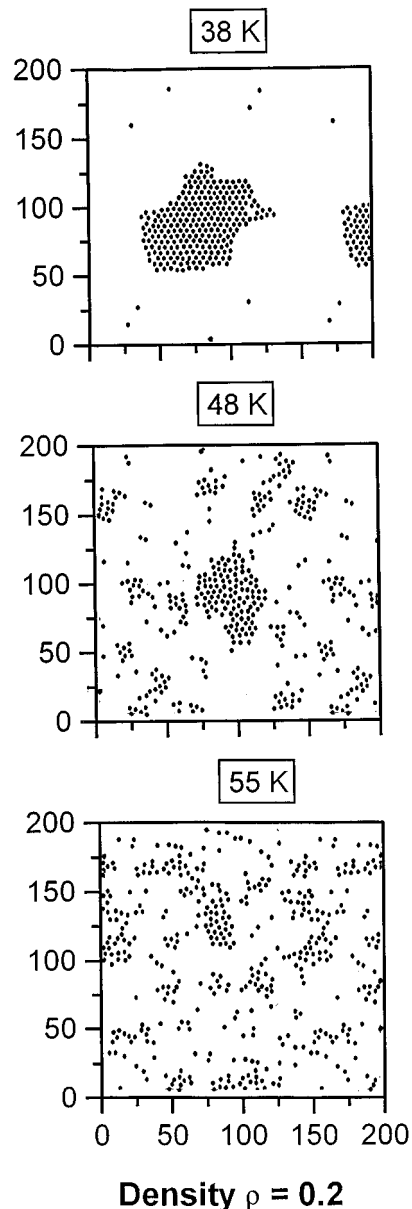


FIG. 8. Typical equilibrium configurations of N_2 mass centers for temperatures 38, 48, and 55 K, at $\rho=0.2$. Units are in Å.

internal energy. Were this condition maintained, the melting temperature would remain at 47 K in the limit of arbitrarily low surface density. However, as the temperature is increased toward melting, the entropy increases if a distribution of smaller island sizes are formed, thus minimizing the Helmholtz free energy. This is just the condensation problem. It has been established that T_M reduces as island sizes decrease.⁵⁶ It is the competition between the internal energy and the entropy, as T approaches T_M , that must be understood.

The character of the specific heats and the order parameters versus ρ give additional insight to the melting phenomenon. In particular, the calculated specific heat peaks change in a nonmonotonic way with ρ , much as observed by experiment.^{21,22} Moreover, this feature seems to occur in many different adlayer systems.^{2,29-32} This behavior has never been satisfactorily explained. To understand it, remem-

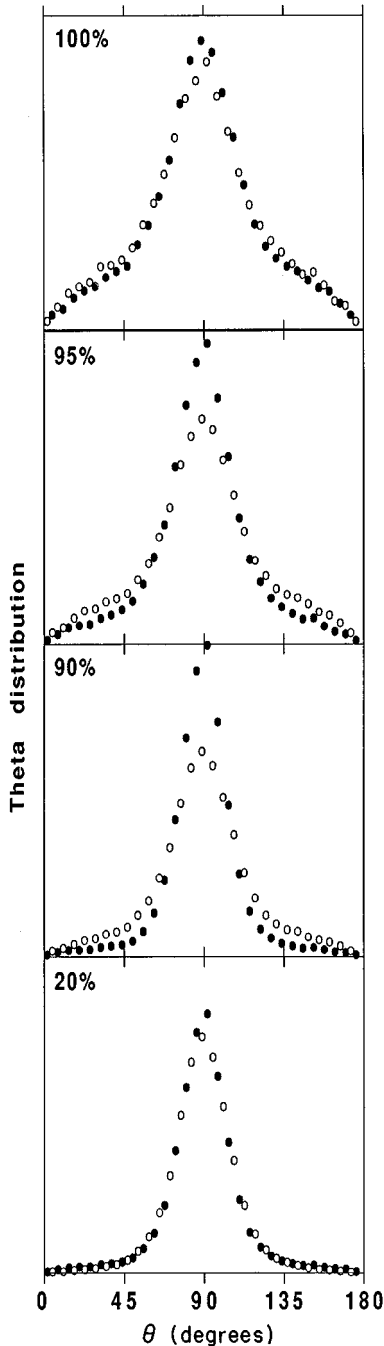


FIG. 9. The probability distribution $P(\theta)$ for the polar angle of N_2 orientations with respect to the z axis, normal to the substrate plane. From top to bottom the surface densities are $\rho=(1.0,0.95,0.9,0.2)$. The solid and open circles represent temperatures (75,95 K), (55,80 K), (35,55 K), and (38,55 K), at these densities, respectively.

ber the specific heat is proportional to $\Delta E/\Delta T$ at constant surface area, where E is the internal energy of the adlayer. A small ΔT leads to a high specific-heat peak height and a narrow width, and vice versa. A large ΔE on transition leads to a high peak height.

At $\rho=1$ the system is uniform with a $\sqrt{3}\times\sqrt{3}$ solid order below T_M , and near melting second-layer promotion creates

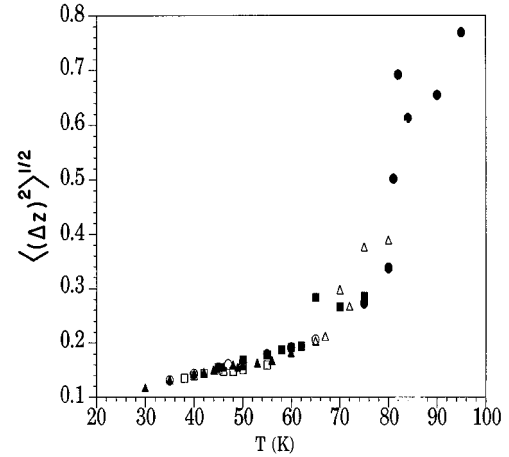


FIG. 10. The rms N_2 mass center fluctuations normal to the substrate vs temperature. The solid circles, open triangles, solid squares, open circles, solid triangles, and open squares represent $\rho=(1.0,0.95,0.93,0.9,0.5,0.2)$, respectively.

vacancies in the monolayer plane that facilitates melting at $T\approx 82$ K. The energy difference between the ordered solid and the disordered fluid is fairly large, as determined directly by our calculations. Moreover, since the solid is nearly uniform, when the thermal energy is sufficient, melting occurs over the entire system in a small interval ΔT . This is supported by the behavior of the order parameters around T_M . Thus, the peak is high and relatively sharp.

For low densities $\rho\leq 0.5$, the specific-heat peak is also narrow and even higher than at $\rho=1$. The key feature is that large solid $\sqrt{3}\times\sqrt{3}$ patches form at low temperatures, surrounded by a void. The local density is very nonuniform, with regions with $\rho=1$ and others with $\rho=0$. The patch edges experience no constraint in the lateral direction due to the void. As a consequence, the behavior of the patches are much as the monolayer examined³⁹ using a constant pressure ensemble, where the surface area can respond to changing thermodynamic conditions. In that case, the specific-heat peak was high and sharp, and the transition was first-order-like. Because the binding energy of the edge molecules is less than those interior, they melt first, rapidly followed by the others. That is, when the temperature is sufficient to dissociate the edge molecules, the patch expands into the void. The interval ΔT is small over the transition from an ordered patch to a low-density fluid as evidenced by the order parameters. Moreover, the calculated ΔE is large because the internal energy of the high-density patch is much greater than the final-state low-density fluid; see Figs. 7 and 8. For $\rho<0.2$, the above arguments compel us to predict the specific-heat peaks will be high and sharp.

At intermediate densities ($\rho=0.95,0.93,0.9$), the solid has many intrinsic vacancies and small voids as the temperature approaches T_M . At this temperature there is not enough thermal energy to populate the second layer. Thus, the solid is partially disordered and nonuniform, as shown by the configurations and the order parameters. The calculated difference ΔE upon transition from the disordered solid to a dense fluid, is small. Moreover, molecules near vacancies and voids initiate melting at a lesser temperature than those im-

bedded in the interior of a $\sqrt{3}\times\sqrt{3}$ region because they are less bound and have space to fluctuate in a lateral direction. That is, because of the nonuniform structure of the solid adlayer near melting, some molecules melt at a lower temperature than others. Thus, ΔT is extended. The result is a shallow, broad specific-heat peak.

It is important to recognize the quantitative accuracy of the results depends greatly upon the description of the interactions. The N_2 - N_2 potential is known to high accuracy,⁴³⁻⁴⁵ but the N_2 -graphite interaction is less reliable. Probably the substrate-mediated dispersion correction⁵³ is of most concern, mostly because of uncertainty in its quantitative accuracy. This correction is rather large if the commonly used parameters are utilized,⁵⁵ as was done in this work. Thus, results compared with and without this term give an approximate bound in the uncertainty. It was found that there is no qualitative difference. There were quantitative differences, as shown in Fig. 3 for the predicted melting temperature, but even those are not major. It is notable this correction has the effect of slightly lower the melting temperature for small ρ and increase it for $\rho\geq 0.9$. For N_2 graphite this term in the potential is repulsive for all densities. At low ρ it is the edge molecules of the patch that initiate melting. The potential well experienced by those molecules, in the local field of the others, has a repulsive barrier that inhibits motion into the patch. But there is a shallow barrier to motion toward the void, because of the dispersion part of the potential. The repulsive mediated dispersion correction contributes by reducing the potential well depth and weakens the long-range dispersion. Thus, the barrier that inhibits fluctuations away from the patch decreases and reduces the temperature required to initiate melting. The situation is quite different at high densities where there are few voids and each molecule experiences a local potential with a repulsive barrier which surrounds the molecule. The repulsive mediated dispersion correction acts to make the walls of the potential well even more repulsive and closer together. This change requires more thermal energy to achieve the same translational fluctuation Δr of the molecules. A qualitative picture of the change in the potential is shown in Fig. 11. In simple terms, the local field is more localized and the temperature must be higher before the amplitude of fluctuations Δr is the same as in a less repulsive potential. Thus, T_m increases.

We note that a great deal of computational effort was expended to bring these systems into equilibrium. The problem is twofold. First, the vacancies are not very mobile and require many configurations to go from the initial state to equilibrium. Second, fluctuation quantities such as the specific heats demand high accuracy. This requirement is particularly important at $\rho=0.9, 0.93,$ and 0.95 , where the specific heat peaks are very small and high accuracy is required to detect them. It was essential to utilize the multiple histogram method to improve efficiency and accuracy. For each ρ , the overlapping probability distributions at eight different temperatures were required. Even so, some 2.5×10^4 cpu hours were required on an IBM 6000 RISC work station. The histogram method is truly a valuable tool.

Finally, we note that many adlayer systems on heterogeneous substrates exhibit qualitatively similar melting curves^{2,29-33} versus ρ . We expect that the quantitative differences depend strongly on the relative strength of the in-

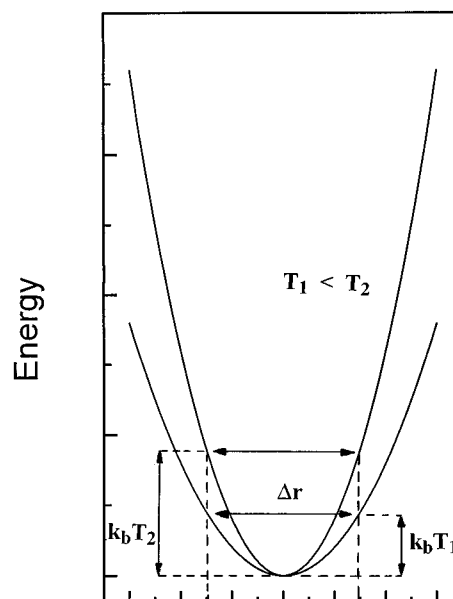


FIG. 11. The shallow parabola depicts qualitatively the total potential experienced by a molecule due to all neighbors near $\rho=1$. The more narrow parabola shows that potential when the repulsive substrate mediated dispersion correction is added. $\Delta T=T_2-T_1$ is the added temperature required to achieve the same rms fluctuation with the correction as without.

out-of-plane forces on the molecules and only weakly on whether or not the system is registered. It remains to be proven how general the arguments of this work are. It should be noted that the term "melting" is used loosely here. At low ρ , probably sublimation is more appropriate. At high density the high-temperature state is fluid, but it is not an ideal liquid.

An article,⁵⁷ published while this manuscript was being processed, uses the molecular-dynamics method to examine the distribution of vacancies at various surface densities. From this some features of melting were postulated. While the results are not accurate enough to determine specific-heat line shapes, many points that are in common between our work^{39,40} and theirs are qualitatively in accord, except the influence of the substrate-mediated dispersion correction on T_M . We find that at $\rho=0.2$ and 0.5 , this correction reduces T_M by only 2-3 K. At higher ρ , the change becomes zero and is positive near monolayer completion. This is quite different than reported by Hansen *et al.*⁵⁷ We conjecture that the differences occur partially because our statistical uncertainty is significantly smaller. Also, their work at $\rho=0.214$ and 0.5 is suspect because the number of molecules used is small, and size effects surely compromise the quantitative results.⁵⁶

ACKNOWLEDGMENT

This work was supported by U.S.-Polish Joint Maria Sklodowska-Curie Fund II MEN/NSF Grant No. 94-163.

- *Permanent address: Institute of Chemical and Theoretical Chemistry, Technical University, Wrocław, Poland.
- ¹F. Abraham, *Phys. Rep.* **80**, 339 (1981).
- ²K. Strandburg, *Rev. Mod. Phys.* **60**, 161 (1988).
- ³J. Kosterlitz and D. Thouless, *J. Phys. C* **6**, 1181 (1973); B. Halperin and D. Nelson, *Phys. Rev. Lett.* **41**, 121 (1978); A. Young, *Phys. Rev. B* **19**, 1855 (1979).
- ⁴D. Frenkel and J. McTague, *Phys. Rev. Lett.* **42**, 1632 (1979).
- ⁵F. Abraham, *Phys. Rev. Lett.* **44**, 463 (1980).
- ⁶F. Abraham, *Phys. Rev. B* **23**, 6145 (1981); S. Koch and F. Abraham, *ibid.* **27**, 2964 (1983).
- ⁷J. Phillips, L. Bruch, and R. Murphy, *J. Chem. Phys.* **75**, 5097 (1981).
- ⁸S. Toxvard, *Phys. Rev. Lett.* **44**, 1002 (1980); **51**, 1971 (1983).
- ⁹E. Domany and E. Riedel, *Phys. Rev. Lett.* **40**, 561 (1978).
- ¹⁰F. Abraham, *Phys. Rev. B* **29**, 2606 (1984).
- ¹¹J. A. Combs, *Phys. Rev. Lett.* **61**, 714 (1988).
- ¹²W. Brinkman, D. Fisher, and D. Moncton, *Science* **217**, 693 (1982).
- ¹³F. Abraham, *Phys. Rep.* **80**, 339 (1981).
- ¹⁴F. Von Swoi, L. Woodcock, and J. Cape, *J. Chem. Phys.* **73**, 913 (1980).
- ¹⁵J. Zollweg and G. Chester, *Phys. Rev. B* **48**, 11 186 (1992).
- ¹⁶R. D. Diehl and S. Fain, *J. Chem. Phys.* **77**, 5065 (1982).
- ¹⁷R. D. Diehl and S. C. Fain, Jr., *Surf. Sci.* **125**, 116 (1983).
- ¹⁸R. D. Diehl, M. F. Toney, and S. C. Fain, Jr., *Phys. Rev. Lett.* **48**, 177 (1982).
- ¹⁹R. D. Diehl and S. C. Fain, Jr., *Phys. Rev. B* **26**, 4785 (1982).
- ²⁰H. You and S. C. Fain, Jr., *Faraday Disc. Chem. Soc.* **80**, 159 (1985).
- ²¹M. H. Chan, A. D. Migone, K. D. Miner, and Z. R. Li, *Phys. Rev. B* **30**, 2681 (1984).
- ²²T. Chung and G. Dash, *Surf. Sci.* **66**, 559 (1977).
- ²³A. Inaba and H. Chihara, *Can. J. Chem.* **66**, 703 (1988).
- ²⁴K. Kjems, L. Passell, H. Taub, J. G. Dash, and A. D. Novaco, *Phys. Rev. B* **13**, 1446 (1976).
- ²⁵W. Brooks (unpublished).
- ²⁶J. Rouquerol, S. Partyka, and F. Rouquerol, *J. Chem. Soc. Faraday Trans. I* **73**, 306 (1977).
- ²⁷J. Piper, J. Morrison, C. Peters, and Y. Ozaki, *J. Chem. Soc. Faraday Trans.* **79**, 2863 (1983).
- ²⁸A. D. Migone, H. Kim, M. Chan, J. Talbot, D. Tidesley, and W. A. Steele, *Phys. Rev. Lett.* **51**, 192 (1983).
- ²⁹J. Laresé, L. Passell, A. Heidemann, D. Richter, and J. Wicksted, *Phys. Rev. Lett.* **61**, 432 (1988).
- ³⁰S. Satija, L. Passell, J. Eckert, W. Ellenson, and H. Patterson, *Phys. Rev. Lett.* **51**, 411 (1983).
- ³¹H. Kim, Q. Zhang, and M. Chan, *Phys. Rev. Lett.* **56**, 1579 (1986).
- ³²A. Cheng and M. Klein, *Langmuir* **8**, 2798 (1992).
- ³³T. Hakim, H. Glyde, and S. Chui, *Phys. Rev. B* **37**, 974 (1988).
- ³⁴V. Joshi and D. Tildesley, *Mol. Phys.* **55**, 999 (1985).
- ³⁵W. Carlos and M. Cole, *Surf. Sci.* **91**, 339 (1980).
- ³⁶F. Hansen and H. Taub, *Phys. Rev. Lett.* **69**, 652 (1992).
- ³⁷J. Talbot, D. Tildesley, and W. Steele, *Faraday Discuss. Chem. Soc.* **80**, 1 (1985); F. Y. Hansen and L. W. Bruch, *Phys. Rev. B* **51**, 2515 (1995).
- ³⁸A. Ostlund and A. Berker, *Phys. Rev. Lett.* **42**, 843 (1979).
- ³⁹R. D. Eters, M. Roth, and B. Kuchta, *Phys. Rev. Lett.* **65**, 3140 (1990); M. Roth and R. D. Eters, *Phys. Rev. B* **44**, 6581 (1991).
- ⁴⁰R. D. Eters, B. Kuchta, and J. Belak, *Phys. Rev. Lett.* **70**, 826 (1993).
- ⁴¹A. M. Ferrenberg and R. H. Swendsen, *Phys. Rev. Lett.* **63**, 1195 (1989).
- ⁴²P. Bowen, J. Burke, P. Corsten, K. Crowell, K. Farrel, J. Macdonald, R. Macdonald, A. MacIsaac, P. Poole, and N. Jan, *Phys. Rev. B* **40**, 7439 (1989).
- ⁴³R. Berns and A. van der Avoird, *J. Chem. Phys.* **72**, 6107 (1980).
- ⁴⁴R. LeSar and R. Gordon, *J. Chem. Phys.* **84**, 5479 (1986).
- ⁴⁵R. D. Eters, J. Belak, and R. LeSar, *Phys. Rev. B* **34**, 4221 (1986); J. Belak, R. D. Eters, and R. LeSar, *J. Chem. Phys.* **89**, 1625 (1988).
- ⁴⁶R. D. Eters, V. Chandrasekharan, E. Uzan, and K. Kobashi, *Phys. Rev. B* **33**, 8615 (1986).
- ⁴⁷J. Belak, R. LeSar, and R. D. Eters, *J. Chem. Phys.* **92**, 5430 (1990).
- ⁴⁸B. Kuchta and R. D. Eters, *Phys. Rev. B* **36**, 3400 (1987).
- ⁴⁹B. Kuchta and R. D. Eters, *J. Chem. Phys.* **88**, 2793 (1987).
- ⁵⁰W. A. Steele, *J. Phys. (Paris) Colloq.* **38**, C4-61 (1978).
- ⁵¹W. A. Steele, *Surf. Sci.* **36**, 317 (1973).
- ⁵²B. Kuchta and R. D. Eters, *Phys. Rev. B* **36**, 3400 (1987).
- ⁵³A. D. McLachlan, *Mol. Phys.* **7**, 381 (1964).
- ⁵⁴S. Rauber, J. Klein, M. Cole, and L. Bruch, *Surf. Sci.* **123**, 173 (1982).
- ⁵⁵B. Kuchta and R. D. Eters, *Phys. Rev. B* **36**, 3400 (1987).
- ⁵⁶S. Kumar, M. Roth, B. Kuchta, and R. D. Eters, *J. Chem. Phys.* **97**, 3744 (1992).
- ⁵⁷F. Y. Hansen, L. W. Bruch, and H. Taub, *Phys. Rev. B* **52**, 8515 (1995).